

# Thermal conductivity in metallic nanostructures at high temperature: Electrons, phonons, and the Wiedemann-Franz law

N. Stojanovic,<sup>1,2,\*</sup> D. H. S. Maithripala,<sup>3</sup> J. M. Berg,<sup>1,2</sup> and M. Holtz<sup>2,4</sup>

<sup>1</sup>*Department of Mechanical Engineering, Texas Tech University, Lubbock, Texas 79409, USA*

<sup>2</sup>*Nano Tech Center, Texas Tech University, Lubbock, Texas 79409, USA*

<sup>3</sup>*Department of Mechanical Engineering, University of Peradeniya, Peradeniya, Kandy 20400, Sri Lanka*

<sup>4</sup>*Department of Physics, Texas Tech University, Lubbock, Texas 79409, USA*

(Received 15 April 2010; revised manuscript received 7 July 2010; published 19 August 2010)

The Boltzmann transport equation is used to calculate thermal and electrical conductivity of metal nanostructures with characteristic dimensions in the 25–500 nm range, near to and above the Debye temperature. Thermal conductivity contributions from phonons and electrons are considered. The intrinsic effects of electron-phonon, phonon-phonon, and phonon-electron scattering, and grain boundary and surface interactions are addressed. Excellent agreement is found between model results and available data reporting direct measurements of thermal conductivity of nanowires, ribbons, and thin films in Al, Pt, and Cu, respectively. The Wiedemann-Franz (W-F) law and Lorenz factor are examined with decreasing size; their applicability is found to degrade in nanowires due mainly to increased relative phonon contribution. The effect of differences in the electron mean-free path for thermal gradient versus electrical field is also examined. A modified version of W-F is presented, corrected for these two factors and valid from macroscale to nanoscale provided characteristic sizes exceed the phonon mean-free path.

DOI: [10.1103/PhysRevB.82.075418](https://doi.org/10.1103/PhysRevB.82.075418)

PACS number(s): 63.22.Gh, 65.80.-g, 73.63.-b

## I. INTRODUCTION

While charge transport in metals is due solely to electrons, heat is carried both by electrons and phonons. The total thermal conductivity  $\kappa$  is the sum of the electronic thermal conductivity,  $\kappa_e$ , and the phonon thermal conductivity,  $\kappa_{ph}$ , along with any other heat-carrying mechanisms when present. In this paper, we focus on  $\kappa_e$  and  $\kappa_{ph}$  in metals, in the so-called high-temperature range near to or above the Debye temperature  $\theta_D$ . In this range, it is generally assumed that  $\kappa_{ph}$  is negligible for metals, and therefore  $\kappa \approx \kappa_e$ . However, this assumption has not been subjected to rigorous experimental verification, particularly at the nanoscale, due to difficulties in direct measurement of  $\kappa_{ph}$ . In metallic structures with nanoscale dimension, both  $\kappa$  and electrical conductivity  $\sigma$  are known to be significantly different from their bulk counterparts,<sup>1</sup> with the observed reductions generally attributed to scattering of electrons and phonons at surfaces and by grain boundaries.<sup>2–4</sup>

There is also experimental evidence that the theoretically predicted relationship between  $\sigma$  and  $\kappa$ , as expressed by the Wiedemann-Franz (W-F) law, breaks down at the nanoscale.<sup>5,6</sup> The neglected  $\kappa_{ph}$  component is one factor that has been cited as contributing to the apparent discrepancy in W-F.<sup>7</sup> Another factor is inelastic electron-phonon scattering that influences transport due to a temperature gradient but not due to an electric field.<sup>8</sup> These hypotheses are plausible but have not been quantitatively tested against experimental data. In this paper, we develop models based on the Boltzmann transport equation (BTE) for size dependence of  $\sigma$  and  $\kappa$  in nanowires with rectangular cross section. The expressions are evaluated numerically. We validate the BTE-based models by comparison with available experimental results for metallic nanostructures. Agreement with direct measurements reported on Al nanowires, Pt nanoribbons, and Cu thin

films is excellent. We use the validated model to predict  $\sigma$ ,  $\kappa_e$ , and  $\kappa_{ph}$  in square nanowires of Au, Ag, Cu, Al, Ni, Pt, and W. There are significant differences between the metals but in general we find that both  $\kappa_{ph}$  and inelastic scattering must be considered.

The remainder of the paper is organized as follows: Sec. II provides a more in-depth background. Section III describes the BTE-based approach to calculating  $\kappa_{ph}$  and  $\kappa_e$  for nanowires with rectangular cross section. Section IV compares the results of the models with available direct measurements of thermal conductivity for rectangular Al nanowires, Pt nanoribbons, and Cu thin films at room temperature (RT). Section IV also applies the results to square nanowires of various standard metals for which experimental data is not available. Section V discusses validity of the W-F law and the Lorenz factor in nanostructures due to both the reduction in  $\kappa_e$  with respect to  $\kappa_{ph}$ , and the mean-free-path inequality. Section VI presents conclusions. The Appendix contains detailed expressions needed to carry out these calculations for other materials, and provides important limiting cases.

## II. BACKGROUND

The Wiedemann-Franz law states that  $\kappa/\sigma = LT$ , where  $L$  is the Lorenz factor and  $T$  is the absolute temperature. Sommerfeld theory suggests that  $L$  should be constant for all metals, and leads to the well-known value,  $L_0 = (\pi^2/3)(k_B/e)^2 = 2.44 \times 10^{-8} \text{ V}^2/\text{K}^2$ , where  $e$  is the elementary charge and  $k_B$  is Boltzmann's constant. However, it has been experimentally established that the Lorenz factor is material and temperature dependent, with bulk values for various metals observed significantly above and below  $L_0$ . This may be seen in Table I, where we summarize published experimental values of selected bulk metals for each of the following quantities: electrical resistivity ( $\rho = 1/\sigma$ ), total

TABLE I. Published experimental values of electrical resistivity, total thermal conductivity, Lorenz factor, Debye temperature, and electron mean-free path for selected metals. All values at 300 K.

Metal	$\rho^{26}$ ( $\times 10^{-8}$ $\Omega$ m)	$\kappa^{26}$ (W/m K)	$L^{26}$ ( $\times 10^{-8}$ $\text{V}^2/\text{K}^2$ )	$\theta_D^{12}$ (K)	$\lambda_e^E$ (nm)
Au	2.20	318	2.37	165	41.7 (Ref. 13)
Ag	1.61	429	2.34	225	52 (Ref. 23)
Cu	1.70	401	2.31	315	39 (Ref. 23)
Al	2.65	237	2.13	396	22 (Ref. 27)
Ni	7.00	90.7	2.15	375	14 (Ref. 5)
Pt	10.4	71.6	2.52	240	23 (Ref. 6)
W	5.30	170	3.05	310	40 (Ref. 28)

thermal conductivity, Lorenz factor, Debye temperature, and electron mean-free path  $\lambda_e$  for selected metals. The  $\kappa_{ph}$  contribution and inelastic electron-phonon scattering are the two main factors that cause  $L$  to deviate from  $L_0$ . We find that  $\kappa_{ph}$  is the larger of these. Since W-F applies to electronic conduction of both charge and heat, it is reasonable to adopt the phonon-corrected Lorenz factor,

$$L_c \equiv \kappa_e/\sigma T = (\kappa - \kappa_{ph})/\sigma T \quad (1)$$

within this interpretation. In the absence of other effects,  $L_c$  should equal  $L_0$ . However, the influence of inelastic scattering will cause  $L_c$  to be less than  $L_0$ . This effect is incorporated by distinguishing between the electron mean-free path under an applied electric field, denoted  $\lambda_e^E$ , and the electron mean-free path under a temperature gradient, denoted  $\lambda_e^{\nabla T}$ .

The relation between the mean-free paths and the Lorenz factors may be shown to be

$$\lambda_e^{\nabla T}/\lambda_e^E \approx L_c/L_0. \quad (2)$$

Bulk values for  $L_c$  and  $\lambda_e^E$  may thus be used in Eq. (2) to estimate  $\lambda_e^{\nabla T}$ . The relative importance of the inelastic process increases as temperature decreases, although the effect is significant in some metals even near and above  $\theta_D$ . In Sec. V, we apply this analysis to the case of metallic nanowires. We find that by incorporating  $L_c$  and  $\lambda_e^{\nabla T}$  with the BTE-based models a version of W-F is obtained which is valid at dimensions ranging from bulk to the nanoscale.

At constant temperature, W-F implies the so-called electron-thermal transport analogy (ETTA),<sup>9</sup>  $\kappa/\kappa_{bulk} = \sigma/\sigma_{bulk}$ , where  $\kappa_{bulk}$  and  $\sigma_{bulk}$  are the bulk conductivities. Along with the W-F correction to  $L_c$  in Eq. (1) is a phonon-corrected form of the ETTA,  $\kappa_e/\kappa_{e,bulk} = \sigma/\sigma_{bulk}$ . The corrected ETTA holds only when inelastic scattering can be neglected. Otherwise even the corrected equation will not provide accurate values for  $\kappa_e$ .

BTE solutions are obtained describing electron and phonon transport in nanowires with rectangular cross sections. Extension of the electron-transport BTE to the nanoscale for both thin films and rectangular nanowires is accomplished using the Fuchs-Sondheimer<sup>2,3</sup> and Mayadas-Schatzkes<sup>4,10</sup> models. A similar approach has been previously reported by Lu *et al.*<sup>11</sup> using asymptotic expansions and truncated series for computing  $\kappa_e$ . In our treatment, we replace these expan-

sions and series with complete integrals. The electron-transport solutions describe the size dependence of  $\sigma$  and  $\kappa_e$ , utilizing the (experimental) bulk values as input. Values used for the electron wave-function reflection coefficient  $R$  and surface specular reflection coefficient  $p_{ph}$  for phonons are consistent with the ranges reported in the literature, as is the choice  $p_e=0$  coefficient due to the short electron wavelengths when compared with typical surface roughness. As mentioned above, the BTE for  $\sigma$  incorporates  $\lambda_e^E$  while that for  $\kappa_e$  incorporates  $\lambda_e^{\nabla T}$ .

The vibrational term  $\kappa_{ph}$  is primarily due to transport by acoustic phonons, due to their high group velocity. The phonon-phonon Umklapp ( $U$ ) process is the dominant scattering mechanism for these phonons at high temperatures. Phonon-electron scattering can also reduce phonon mean-free path,  $\lambda_{ph}$ . For most materials, the latter effect is seen only at low temperature but for transition metals, it can be important at temperatures near  $\theta_D$ , due to the high valence-electron density of states.<sup>12</sup>

We find that in general, both mechanisms must be included in order to obtain satisfactory results. The  $\kappa_{ph}$  model predicts the size dependence and the value. No new adjustable parameters are introduced, and values obtained for previously introduced parameters are in good agreement with published work. Experimental measurements of  $\kappa_{ph}$  are not available, although our values are in accord with theoretical estimates of  $\kappa_{ph}$  obtained by molecular dynamics (MD) simulations.<sup>13-15</sup>

Total thermal conductivity may now be modeled as follows: the  $\kappa_{ph}$  model is used to find  $\kappa_{ph,bulk}$ , and thus  $\kappa_{e,bulk}$  from the measured bulk total thermal conductivity. Then  $\kappa_{e,bulk}$  is used with the BTE size-dependent model to give  $\kappa_e$  as a function of nanowire dimension. Finally the BTE value of  $\kappa_{ph}$  is added to give total  $\kappa$  as a function of nanowire dimension. The resulting  $\kappa$  values are validated against reported direct measurements on rectangular Al nanowires, Pt nanoribbons, and Cu thin films, with excellent agreement. The model is also used to generate total  $\kappa$  for square nanowires of various metals and cross section. The models predict that typically, as the wire dimensions decrease  $\kappa_e$  undergoes significant reduction while  $\kappa_{ph}$  remains nearly constant. This agrees with results of recent experiments on Al nanowires.<sup>16</sup> The reduction in  $\kappa_e$  is attributed to  $\lambda_e$  being greater than  $\lambda_{ph}$ , a situation that generally holds in metals. The resulting large

reduction in  $\kappa_e$  relative to  $\kappa_{ph}$  suggests that the practice of neglecting  $\kappa_{ph}$  in metals must be revisited at the nanoscale.

### III. BTE CALCULATION OF $\kappa_{ph}$ AND $\kappa_e$ FOR RECTANGULAR NANOWIRES

In this section, we extend previous approaches to solution of the BTE for electron and phonon transport, and provide theoretical expressions for  $\sigma$ ,  $\kappa_e$ , and  $\kappa_{ph}$  for metal nanowires having rectangular cross section of width  $a$  and thickness  $b$ . The expressions are suitable for numerical evaluation.

We distinguish between the “confined” directions of width and thickness, and the “unconfined” direction of length. The following assumptions are required: (a) materials are isotropic and the nearly free electron model holds. We restrict our interest to length scales for which quantum confinement of electrons or phonons is not a factor. (b) The Debye approximation for phonons holds. (c) There is no temperature gradient  $\nabla T$  or electric field  $E$  along the confined directions, and either  $\nabla T$  or  $E$  is applied along the unconfined direction. The magnitude of  $\nabla T$  or  $E$  is small enough that the assumption of small perturbation holds. (d) The material exists in a perturbed state near equilibrium, with local distributions of electrons and phonons governed by the BTE under the relaxation-time approximation (RTA). (e) The local electron and phonon distributions explicitly depend on position in the confined directions but do not explicitly depend on position in the unconfined direction.

#### A. Phonon thermal conductivity

The phonon contribution to  $\kappa$  is modeled by solving the BTE for the nonlinear acoustic-phonon distribution, applying Fuchs’ boundary condition of partially specular scattering at the surfaces.<sup>2</sup> Parameter  $p_{ph}$  corresponds to the probability a phonon incident on a surface will scatter specularly. Here, it should be noted that surface roughness plays the dominant role in determining phonon surface specularity. For near-normal incidence, it may be approximated  $p_{ph} = \exp(-16\pi^3 \eta^2 / \Lambda^2)$ ,<sup>17</sup> where  $\eta$  is the surface roughness and  $\Lambda$  is phonon wavelength. As seen from this expression, each phonon will have different  $p_{ph}$  depending on the wavelength. To account for this dependence, we estimate the average  $p_{ph}$  by weighting with the acoustic-phonon density of states, the Bose function, and the phonon mean-free path, with average value  $\sim 0.5$  discussed below. As expected, acoustic phonons from the Brillouin-zone center ( $q < q_{max}/5$ ) are emphasized by this weighting approach. This is reasonable since long-wavelength acoustic phonons are primarily responsible for heat transport. Furthermore, these phonon wavelengths are well in excess of the dimension of the grain boundary. Thus, vibrations are expected to propagate from one grain into another without substantial reflection; in our model we do not include the wave reflection coefficient of phonons at grain boundaries.

Letting  $\tau_{ph}$  represent the phonon relaxation time,  $q$  the phonon wave vector, and  $v_\beta$  the velocity of acoustic phonons in branch  $\beta$ , the phonon thermal conductivity is

$$\kappa_{ph}(p_{ph}, T, a, b) = \frac{\kappa_B^4}{6\pi^2 \hbar^3} T^3 \sum_\beta \frac{1}{v_\beta} \int_0^{\Theta_D} \left\{ \tau_{ph}(s) \frac{s^4 e^s}{(e^s - 1)^2} \times [1 - g_{ph}(p_{ph}, \tau_{ph}(s), v_\beta, a, b)] \right\} ds, \quad (3)$$

where  $\omega_\beta = v_\beta q$  and integration variable  $s = \hbar \omega_\beta(q) / k_B T$ . Size dependence is captured by function  $g_{ph}$ , which is Eq. (A2) in the Appendix. Prior work has computed  $g_{ph}$  for nanowires with circular cross section, using a quadratic approximation of the phonon dispersion.<sup>18</sup> Additional effects on the phonon dispersion due to confinement have been investigated,<sup>19</sup> and extended to rectangular nanowires based on expressions in the forms of asymptotic expansions.<sup>11</sup> The present paper retains full expressions for integrals appearing in the solutions, rather than approximating them with asymptotic expansions and truncated infinite series.

We incorporate phonon-phonon and phonon-electron scattering into the relaxation time  $\tau_{ph}$ . To account for multiple factors, the individual scattering rates are summed according to Matthiessen’s rule. The  $U$  processes are assumed to be the dominant phonon-phonon mechanism, with scattering rate  $\tau_U$  satisfying<sup>20</sup>

$$\frac{1}{\tau_U} = \frac{\hbar \gamma^2}{M v_\beta^2 \theta_D} \omega_{\beta k}^2 T \exp\left(\frac{-\theta_D}{3T}\right), \quad (4)$$

where  $\gamma$  is the Grüneisen parameter<sup>21</sup> and  $M$  is the mass of the unit cell.

Phonon-electron scattering rates are obtained from Klemens and Williams.<sup>12,22</sup> This effect is generally important at low temperatures, and can also be significant at higher temperatures in transition metals because of their high density of electronic states. We find that in general this mechanism must be included in order to obtain satisfactory results. Equation (3) requires no tuning of adjustable parameters. This is important because no direct experimental measurements are available for  $\kappa_{ph}$ .

In the limit  $b \gg a$ , we obtain Eq. (A5) for  $\kappa_{ph}$  of thin films. If  $a$  and  $b$  are both much larger than  $\lambda_{ph}$ , or if the surface scattering is completely specular ( $p_{ph} = 1$ ), then  $g_{ph} \rightarrow 0$ , and we recover Eq. (A6), the well-known result for bulk materials. To validate our relaxation-time model we use Eq. (A6) to predict  $\kappa_{ph}$  for various bulk metals, as summarized in Table II. In the absence of experimental results for  $\kappa_{ph}$ , we compare our results with available published MD values, with reasonable overall agreement.

#### B. Electronic thermal and electrical conductivity

Electronic transport properties for obtaining  $\sigma$  and  $\kappa_e$  are computed by extending the Fuchs-Sondheimer<sup>3</sup> and Mayadas-Schatzkes<sup>4</sup> models for thin films. Applying the listed assumptions (a)–(e), the BTE may be solved for the nonequilibrium electron distribution function, employing Fuchs’ boundary conditions.<sup>2</sup> Grain-boundary scattering effects are taken into account using the Mayadas-Schatzkes<sup>10</sup>

TABLE II. Calculated values for  $\kappa_{ph}$  from Boltzmann transport equation compared with available published calculations from molecular dynamics.

Metal	$\kappa_{ph}$ (BTE) (W/m K)	$\kappa_{ph}$ (MD) (W/m K)
Au	5	4.1 (Ref. 14)
Ag	9.3	7.7 (Ref. 14)
Cu	22.2	18 (Ref. 29)
Al	21.1	21 (Ref. 15)
Ni	9.6	15.8 (Ref. 14)
Pt	8.3	11.7 (Ref. 14)
W	42.2	

assumption of a single electron wave-function reflection coefficient  $R$ . Unlike Eq. (3), which provides a parameter-free estimate of  $\kappa_{ph}$ , the models of  $\sigma$  and  $\kappa_e$  will give only the size-dependent change in the property with respect to the bulk. The bulk electrical conductivity is directly measured. Thus we obtain

$$\sigma = \sigma_{bulk} \{ \Phi(\alpha^E) - g_e(p_e, \alpha^E, \gamma_a^E, \gamma_b^E) \}. \quad (5)$$

The bulk value of  $\kappa_e$  is found from the experimentally measured bulk  $\kappa$ , and  $\kappa_{ph,bulk}$  computed from the bulk limit of Eq. (3),

$$\begin{aligned} \kappa_e &= \kappa_{e,bulk} \{ \Phi(\alpha^{\nabla T}) - g_e(p_e, \alpha^{\nabla T}, \gamma_a^{\nabla T}, \gamma_b^{\nabla T}) \} \\ &= (\kappa_{bulk} - \kappa_{ph,bulk}) \{ \Phi(\alpha^{\nabla T}) - g_e(p_e, \alpha^{\nabla T}, \gamma_a^{\nabla T}, \gamma_b^{\nabla T}) \}. \end{aligned} \quad (6)$$

Scaling affects both  $\Phi$ , which accounts for grain-boundary scattering, and  $g_e$ , which accounts for scattering from the nanowire surface.  $\Phi$  is the well-known expression accounting for grain-boundary scattering in bulk electrical conductivity,<sup>4</sup>

$$\Phi(\alpha) = 3 \left\{ \frac{1}{3} - \frac{1}{2}\alpha + \alpha^2 - \alpha^3 \ln \left( 1 + \frac{1}{\alpha} \right) \right\}. \quad (7)$$

The composite parameter  $\alpha = \frac{\lambda_e R}{d_g (1-R)}$  incorporates the grain size,  $d_g$ , electron mean-free path,  $\lambda_e$ , and grain-boundary reflection coefficient,  $R$ . The function  $g_e(p_e, \alpha, \gamma_a, \gamma_b)$  in Eqs. (5) and (6), which is described in more detail in the Appendix, accounts for finite-size factors. Here  $\gamma_a = a/\lambda_e$ ,  $\gamma_b = b/\lambda_e$  and  $p_e$  is the probability of specular reflection of electrons at the surface. The size of the wire enters through  $d_g$ , which decreases with decreasing dimension. In the bulk limit,  $\Phi \rightarrow 1$  and  $g_e \rightarrow 0$ .

The size-dependent portions of Eqs. (5) and (6) require knowledge of  $\lambda_e^E$  and  $\lambda_e^{\nabla T}$ , respectively. Literature values of  $\lambda_e^E$  are included in Table I. To compute  $\lambda_e^{\nabla T}$ , we use Eqs. (1) and (3) to compute the bulk value of  $L_{c,bulk}$ , and then Eq. (2) as  $\lambda_e^{\nabla T} = (L_{c,bulk}/L_0)\lambda_e^E$ . In Eqs. (5) and (6), we use superscripts to distinguish between parameter values due to thermal gradient, that is,  $\gamma_a^{\nabla T}$ ,  $\gamma_b^{\nabla T}$ , and  $\alpha^{\nabla T}$ , and those due to electric field, that is,  $\gamma_a^E$ ,  $\gamma_b^E$ , and  $\alpha^E$ , with the definitions of the corresponding quantities in the preceding paragraph without the subscripts.

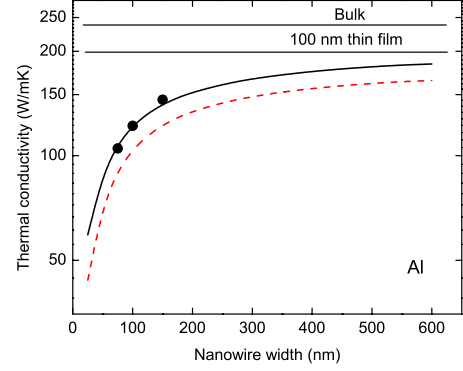


FIG. 1. (Color online) Thermal conductivity of Al nanowires (Ref. 16) with 100 nm thickness and varied width. Dashed curve is for electrons only, solid curve is combined electrons and phonons. Also shown as horizontal lines are measured values of  $\kappa$  for bulk (Ref. 26) and 100-nm-thick film of Al (Ref. 25).

Except for a factor of  $L_0 T$ , Eqs. (5) and (6) are identical functions of the mean-free path. Thus, if  $\lambda_e^E = \lambda_e^{\nabla T}$ , the quantities in brackets will cancel when examining the ratio  $\kappa_e/\sigma$ . In this case,  $\kappa_e/\sigma = L_0 T$ , and the phonon-corrected ETTA is recovered. As discussed above, inelastic electron-phonon scattering typically results in  $\lambda_e^E > \lambda_e^{\nabla T}$ . Then both the Lorenz factor and the ETTA require size-dependent correction terms.

In the thin-film limit,  $b \gg a$  and  $b > \lambda_e$ , we obtain Eq. (A10). When both  $a$  and  $b$  are much greater than  $\lambda_e^{\nabla T}$ , the expressions for bulk  $\sigma$  and  $\kappa_e$  are obtained from Eqs. (5) and (6), respectively, by setting  $g_e = 0$ .

#### IV. RESULTS FOR NANOWIRES, NANORIBBONS, AND THIN FILMS

In this section, we use Eqs. (3) and (6), and their thin film limits Eqs. (A5) and (A10), to calculate room-temperature thermal conductivity for rectangular Al nanowires, Pt nanoribbons, and Cu thin films. These choices are guided by the availability of direct measurements of thermal conductivity, thereby serving as a means to validate our results. In addition, we compute analogous quantities for square nanowires composed of a range of metals.

Figure 1 compares results of Eqs. (3) and (6) to direct measurements of  $\kappa$  for rectangular Al nanowires.<sup>16</sup> The thickness in each case is reported to be 100 nm, and the width varied from 75 to 150 nm. Grain sizes are estimated from scanning electron microscope (SEM) images of the nanowires. The measurements show the expected decrease in thermal conductivity as nanowire cross section decreases. The dashed curve corresponds to the  $\kappa_e$  contribution to  $\kappa$ , obtained from Eq. (6). The calculated result consistently shows  $\kappa_e$  alone to underestimate the total thermal conductivity; the difference has been attributed to the phonon contribution. We calculate  $\kappa_{ph}$  according to Eq. (3), and the net result  $\kappa = \kappa_e + \kappa_{ph}$  is shown as the solid curve in Fig. 1. Agreement between calculated and measured thermal conductivity is excellent. As noted above, in calculating  $\kappa_{ph}$  we assume that there is no grain-boundary scattering of long-wavelength acoustic phonons and use only the phonon sur-

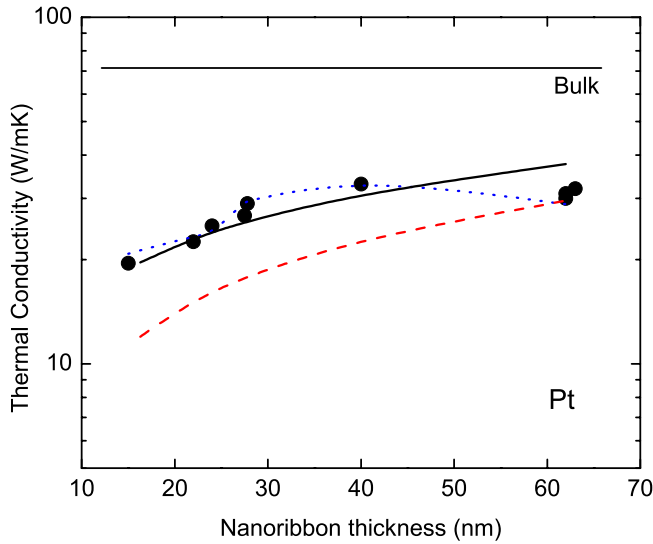


FIG. 2. (Color online) Thermal conductivity of Pt nanoribbons (Ref. 6). Dashed curve is calculated thermal conductivity due to electrons, solid curve is for electrons and phonons. The dotted curve is calculated  $\kappa$  using reported Pt grain sizes. Also shown is the measured value of  $\kappa$  for bulk Pt (Ref. 26).

face specularity ratio as parameter. Using root-mean-squared roughness of  $\eta \sim 3$  nm from our SEM images, we obtain an average value of  $p_{ph} \sim 0.5$ . In contrast, calculating  $\kappa_e$  involves diffusive surface scattering of electrons ( $p_e = 0$ ) and the grain-boundary reflection coefficient  $R$ . We find this parameter by fitting Eq. (5) to the precise electrical conductivity measurements and obtain value of  $R = 0.59$ , close to the previously published results for Al,<sup>23,24</sup> and this parameter is unchanged in calculating  $\kappa_e$ .

It is evident from the results for Al presented in Fig. 1 that the electronic part of the thermal conductivity drops dramatically with decreasing dimension. Over this same range  $\kappa_{ph}$  values, which correspond to the difference between the dashed and solid curves, decrease only slightly. As nanowire width increases, the modeled  $\kappa$  approaches published values for Al films with 100 nm thickness.<sup>25</sup>

Figure 2 compares the calculated  $\kappa$  for Pt nanoribbons to published values based on direct measurements.<sup>6</sup> The ribbon thickness  $a$  ranges from 15 to 63 nm and width  $b$  is in the 262 to 1228 nm range. For these values,  $b \gg a \geq \lambda_e$  so that these structures approximate thin films. As in Fig. 1, we show only the  $\kappa_e$  contribution to total thermal conductivity (dashed curve) and the net result when phonons are considered (solid curve). Parameters  $p_{ph}$  and  $R$  are the same as discussed for Al. Grain size is treated in two ways. For the dashed curve, we have used the standard approximation  $d_g = a/2$ , which gives good general agreement between the calculated trend and the data. For the dotted curve, the estimated grain sizes reported for each ribbon investigated is used in our calculation.<sup>6</sup> Here excellent agreement is obtained, showing the value of using experimentally measured grain size.

Figure 3 compares predicted and directly measured  $\kappa$  values for Cu thin films of varying thickness.<sup>7</sup> Again, the dashed curve is the calculated electronic component only, and the

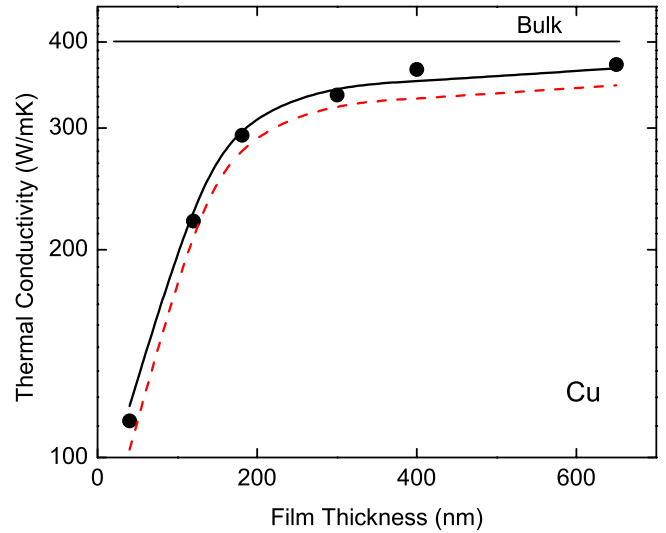


FIG. 3. (Color online) Measured thermal conductivity of Copper thin films (Ref. 7). Dashed curve is for electrons only, solid curve is for electrons and phonons combined. The measured bulk value of  $\kappa$  is also shown for Cu (Ref. 26).

solid curve includes  $\kappa_{ph}$ . The total  $\kappa$  drops rapidly below thickness of  $\sim 200$  nm. The calculated trend agrees well with the data, particularly in the low-thickness range. Since the phonon contribution to the total  $\kappa$  is small for Cu ( $< 6\%$  for the bulk) the dependence is primarily described by  $\kappa_e$ . The agreement between measurement and calculation is excellent.

We also investigate the scaling of  $\kappa_{ph}$  and  $\kappa_e$  with decreasing dimension, using nanowires having square cross section  $a = b$  ranging from 500 to 25 nm. For all calculations,  $d_g \approx a/2$ ,  $R = 0.5$ , electron scattering is assumed completely diffuse at surfaces, and  $p_{ph} = 0.5$ . This choice of parameters is consistent with the ranges reported in the literature for each quantity. Results are summarized in Figs. 4 and 5.

We consider two groups of metals. As seen in Figs. 4(a) and 4(b), Au, Ag, and Cu are characterized by relatively large bulk values of  $\kappa_e$  while for Al, Pt, Ni, and W, these values are significantly smaller. As seen in Figs. 4(c) and

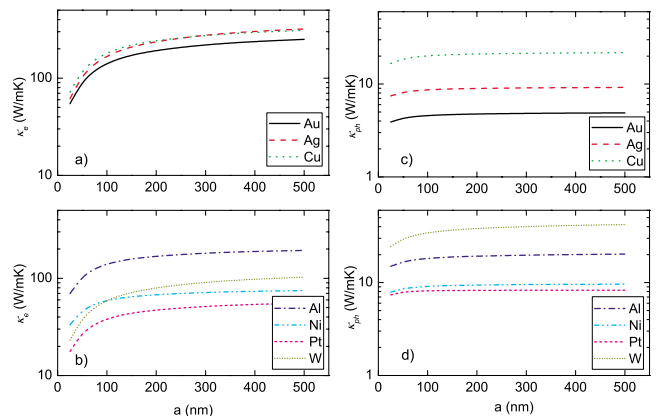


FIG. 4. (Color online) Thermal conductivity of selected metallic nanowires with square cross section at room temperature. (a) and (b)  $\kappa_e$ , (c) and (d)  $\kappa_{ph}$ .

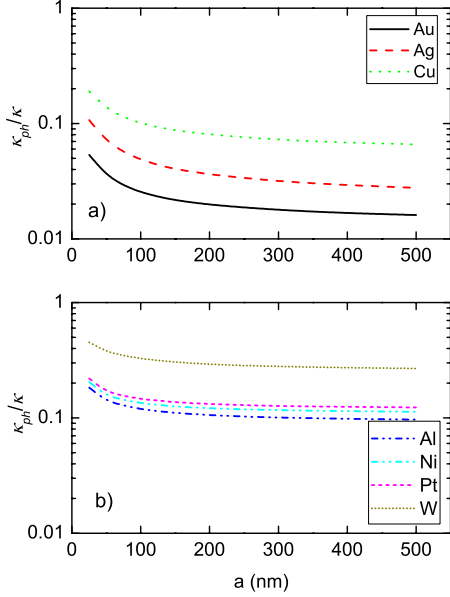


FIG. 5. (Color online) Ratio of phonon to total thermal conductivity for metallic nanowires with square cross section at room temperature.

4(d), both groups show a comparable range of bulk values for  $\kappa_{ph}$ . Thus, as seen in Fig. 5, the fraction of bulk  $\kappa$  attributable to phonons,  $\kappa_{ph}/(\kappa_e + \kappa_{ph})$ , is much smaller for the first group than for the second group. We infer from this that application of W-F for the second group of metals is especially unreliable, and that direct experimental examination of thermal conductivity of these materials is necessary. In all metals considered here,  $\kappa_e$  and  $\kappa_{ph}$  drop from their bulk values as  $a$  decreases. This is due to enhanced scattering of electrons or phonons as the characteristic lengths  $a$  and  $d_g$  approach the electron or phonon mean-free path, respectively. However,  $\lambda_{ph}$  is shorter than  $\lambda_e$  for metals in the high-temperature range, causing the drop in  $\kappa_{ph}$  to occur at smaller  $a$ , and to be less pronounced over the size range considered.

Physically, the difference in scaling behaviors of  $\kappa_{ph}$  and  $\kappa_e$  leads to an increased ratio of  $\kappa_{ph}$  to total  $\kappa$  as  $a$  decreases. As seen in Fig. 5, Au, Ag, and Cu, which have  $\lambda_e$  several times longer than  $\lambda_{ph}$ , and low bulk phonon contributions, show a greater increase in this ratio than Al, Pt, Ni, and W, for which  $\lambda_e$  and  $\lambda_{ph}$  are comparable. In Sec. IV, we explore the implications of these results for the Lorenz factor of these metals in the room-temperature range.

## V. THE LORENZ FACTOR FOR ROOM TEMPERATURE METAL NANOWIRES

As mentioned above, the two main reasons for the breakdown of the W-F law at the nanoscale are increased contribution of  $\kappa_{ph}$  relative to  $\kappa_e$ , and differences between  $\lambda_e^{\nabla T}$  and  $\lambda_e^E$ . To address the first of these factors, we adopt the phonon-corrected Lorenz number,  $L_c$ , defined in Eq. (2).

In the absence of other effects,  $L_c$  should equal  $L_0$ . However, the effect of  $\lambda_e^{\nabla T} \neq \lambda_e^E$  can be seen in Table I, which shows that for many bulk metals at RT,  $L$  is smaller than  $L_0$ .

TABLE III. Corrected value of Lorenz factor and ratio between  $\lambda_e^{\nabla T}$  and  $\lambda_e^E$ .

Metal	$L_c$ ( $\times 10^{-8} \text{ V}^2/\text{K}^2$ )	$\lambda_e^{\nabla T}/\lambda_e^E$
Au	2.33	0.96
Ag	2.29	0.94
Cu	2.18	0.89
Al	1.94	0.79
Ni	1.90	0.78
Pt	2.27	0.93
W	2.30	0.94

From Eq. (1),  $L$  must be greater than  $L_c$  by the amount of  $\kappa_{ph}/\sigma T$ , implying that  $L_c$  is strictly less than  $L_0$ . As discussed, this difference is due to inelastic electron-phonon interactions that scatter electrons from the  $\sim k_B T$  energy range above the Fermi level to just below  $E_F$ . This reduces  $\lambda_e^{\nabla T}$  without affecting  $\lambda_e^E$ , leading to  $\lambda_e^{\nabla T} < \lambda_e^E$ . The inelastic scattering has temperature dependence,<sup>12,26</sup>

$$L_c = L_0 \left[ 1 + \alpha \left( \frac{\theta_D}{T} \right)^2 \right]^{-1}, \quad (8)$$

where  $\alpha = \frac{3}{\pi^2} \left( \frac{2}{Z} \right)^{2/3}$  and  $Z$  is the valence. Metals with  $\theta_D$  below RT will not show a large effect from Eq. (8) so that  $L_c$  is expected to be close to  $L_0$ . When  $\theta_D$  is comparable or higher than RT,  $L_c$  will diminish significantly. Table III summarizes the calculation of  $L_c$  for various bulk metals using Eq. (1) and the value of  $\kappa_{ph}$  from Eq. (A6). The amount by which  $L_c$  is less than  $L_0$  indicates the importance of inelastic scattering for that metal at RT. All materials considered are affected to some extent, particularly for Al and Ni, although at RT this effect remains small. In metals with small Fermi energy, this interpretation is not complete because of so-called Fermi smearing<sup>12,26</sup> but we consider this factor negligible at RT.

To examine the importance at RT of the electron mean-free-path difference, we use Eq. (2) to estimate  $\lambda_e^{\nabla T}/\lambda_e^E$  based on the measured values of  $\lambda_e^E$  in Table I and  $L_c$  from Table III. Results are summarized in Table III. The size-dependent terms in Eqs. (5) and (6) show significant differences due to  $\lambda_e^E \neq \lambda_e^{\nabla T}$  only at sample length scales on the order of  $\lambda_e^E$  and  $\lambda_e^{\nabla T}$  or below. The inequality  $\lambda_e^E > \lambda_e^{\nabla T}$  means that  $\sigma$  will begin to drop before  $\kappa_e$  as size decreases. This causes the change in  $L_c$  and the breakdown of W-F at the nanoscale.

We examine the size dependence of Lorenz factor in nanowires with square cross section ranging from 25 to 500 nm. We calculate  $\sigma$  and  $\kappa_e$  using Eqs. (5) and (6), respectively, with  $\lambda_e^E$  and  $\lambda_e^{\nabla T}$  taken into account using Table III and Eq. (2). Equation (3) is used to find  $\kappa_{ph}$ . Parameters are taken to be the same as for calculations in Fig. 4. Figure 6 shows the resulting Lorenz numbers. The Lorenz factor is seen to rise for  $a=b < 100$  nm. The rise is as large as a factor of 1.5 for narrow (25 nm) nanowires of tungsten. Smaller change is seen in Au and Ag primarily because  $\kappa_{ph}$  remains relatively small compared to the total  $\kappa$ . Generally we find that  $\kappa_{ph}$  is the more important of the two factors considered here, with

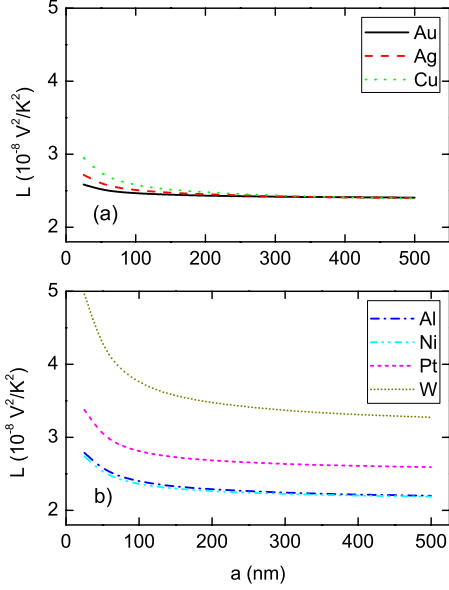


FIG. 6. (Color online) Size dependence of Lorenz factor due to  $\lambda_e^{\nabla T} \neq \lambda_e^E$  and  $\kappa_{ph}$ .

<10% arising from the mean-free-path inequality at length scales  $a=b=25$  nm. However, it is clear that the application of the unmodified W-F law to estimate thermal conductivity for nanowires at this length scale will introduce significant error, even at room temperature. Accounting for both  $\kappa_{ph}$  and the implications of  $\lambda_e^E \neq \lambda_e^{\nabla T}$  are necessary when estimating thermal conductivity based on electrical resistivity.

## VI. SUMMARY

We have presented a BTE-based calculation of electrical and thermal conductivity in metallic nanowires with rectangular cross section. Factors taken into account are phonon-phonon, electron-phonon, and phonon-electron scattering, as well as grain boundary and surface interactions. Previous work on this problem is improved through more complete numerical treatment of the BTE solutions. We use these results to examine the hypothesis that breakdown in the classical Wiedemann-Franz law for nanoscale structures is due to the phonon contribution to the thermal conductivity, and a smaller effect due to the difference between  $\lambda_e^{\nabla T}$  and  $\lambda_e^E$  due to inelastic electron-phonon scattering. We numerically compute  $\kappa_{ph}$ , as well as the geometrical factors affecting  $\kappa_e$ , and  $\sigma$  for selected metals with characteristic dimensions from 25 nm to 500 nm. Results of the calculations for thermal conductivity are shown in Fig. 4. The approach agrees extremely well with direct measurements reported in the literature. Our calculations show significantly higher values for Lorenz number and breakdown of the W-F law at the nanoscale. We find that this breakdown is mainly due to the influence of  $\kappa_{ph}$ , as seen in Fig. 5. However, the difference in electron mean-free path under thermal gradient versus electric field, while much smaller, is still potentially important. Computed values for the Lorenz factor, which may be used for estimating thermal conductivity from electrical resistivity measurements, are summarized in Fig. 6.

## APPENDIX: BTE-BASED CALCULATION OF $\kappa_{ph}$ AND $\kappa_e$

Here we summarize the calculation of the phonon and electronic contribution of the thermal conductivity in metallic nanowires using the BTE. We also report the thin-film limit. In the standard BTE-based approach to computing transport properties, one considers microscopically large but macroscopically small regions in the material and assumes that a local equilibrium density of thermal carriers can be defined. In the presence of an electric field or a temperature gradient, each region is assumed to be near its respective equilibrium and the perturbed densities are assumed to evolve according to the RTA. The key ingredients needed in these computations are the dispersion relationship of the carriers, and the near-equilibrium distribution functions. In the bulk, it is typical to assume that the near-equilibrium distribution functions do not explicitly depend on position, the electronic bands are nearly parabolic, the Fermi surface is spherical, and the Debye approximation holds for phonons. Here we consider characteristic dimensions of 25 nm and greater. At these scales, the effect of finite size on the electronic and vibrational band structures may be neglected. However, the carrier distribution functions are affected by scattering at the free surfaces, and therefore depend on position in the confinement directions. In polycrystalline materials at these scales, there is a reduction in grain size that contributes to an increase in grain-boundary scattering. Incorporating these effects, we compute the lattice and electronic part of thermal conductivity in metallic nanowires and thin films. The derivation follows the work of Mayadas and Fuchs.<sup>2,4</sup>

We first compute the phonon thermal conductivity of a rectangular wire of thickness  $a$  and width  $b$ . Letting  $\tau_{ph}$  be the phonon relaxation time,  $v_\beta$  the Debye velocity of phonons of branch  $\beta$ , and  $p_{ph}$  the specularity parameter of phonon scattering at free surfaces, we have

$$\kappa_{ph} = \frac{\kappa_B^4}{6\pi^2\hbar^3} T^3 \sum_\beta \frac{1}{v_\beta} \int_0^{\Theta_{D/T}} \times \left\{ \tau_{ph}(s) \frac{s^4 e^s}{(e^s - 1)^2} \times [1 - g_{ph}(p_{ph}, \tau_{ph}, v_\beta, a, b)] \right\} ds, \quad (\text{A1})$$

where  $g_{ph}(p_{ph}, \tau_{ph}, v_\beta, a, b)$  captures the size dependence,

$$\begin{aligned} g_{ph}(p_{ph}, \tau_{ph}, v_\beta, a, b) &= \frac{1}{ab} \int_0^b \int_0^a \left\{ \int_{\theta_1}^{\theta_2} S_{ph} \left( p_{ph}, \tau_{ph}, v_\beta, \frac{-y}{\sin \theta}, \frac{-b}{\sin \theta} \right) d\theta \right. \\ &+ \int_{\theta_2}^{\theta_3} S_{ph} \left[ p_{ph}, \tau_{ph}, v_\beta, \frac{(a-x)}{\cos \theta}, \frac{a}{\cos \theta} \right] d\theta \\ &+ \left. \int_{\theta_3}^{\theta_4} S_{ph} \left[ p_{ph}, \tau_{ph}, v_\beta, \frac{(b-y)}{\sin \theta}, \frac{b}{\sin \theta} \right] d\theta \right\} dx dy \end{aligned}$$

$$+ \int_{\theta_4}^{\theta_1} S_{ph} \left( p_{ph}, \tau_{ph}, v_{\beta}, \frac{-x}{\cos \theta'}, \frac{-a}{\cos \theta} \right) d\theta \Bigg\} dx dy \quad (\text{A2})$$

with

$$\begin{aligned} S_{ph}(p_{ph}, \tau_{ph}, v_{\beta}, q, r) &= (1 - p_{ph}) \frac{3}{2\pi} \int_0^{\pi/2} \sin \phi \cos^2 \phi \left( \frac{e^{q/\tau_{ph} v_{\beta} \sin \phi}}{1 - p_{ph} e^{r/\tau_{ph} v_{\beta} \sin \phi}} \right) d\phi \\ &= (1 - p_{ph}) \frac{3}{2\pi} \int_1^{\infty} \frac{\sqrt{u^2 - 1}}{u^4} \left( \frac{e^{qu/\tau_{ph} v_{\beta}}}{1 - p_{ph} e^{ru/\tau_{ph} v_{\beta}}} \right) du \end{aligned} \quad (\text{A3})$$

and geometric parameters,

$$\begin{aligned} \theta_1 &= \arctan \frac{b-y}{a-x}, & \theta_2 &= \pi - \arctan \frac{b-y}{x}, \\ \theta_3 &= \pi + \arctan \frac{y}{x}, & \theta_4 &= -\arctan \frac{y}{a-x}. \end{aligned} \quad (\text{A4})$$

For thin films of thickness  $a$ , it can be shown that

$$\begin{aligned} g_{ph}(p_{ph}, \tau_{ph}, v_{\beta}, a) &= (1 - p_{ph}) \tau_{ph} v_{\beta} \frac{6}{\pi a} \left( \int_0^{\pi/2} \int_0^{\pi/2} \right. \\ &\quad \left. \times \cos \theta \sin^2 \phi \cos^2 \phi \frac{1 - e^{-a/\tau_{ph} v_{\beta} \sin \phi \cos \theta}}{1 - p_{ph} e^{-a/\tau_{ph} v_{\beta} \sin \phi \cos \theta}} d\phi d\theta \right). \end{aligned} \quad (\text{A5})$$

If the nanowire cross-sectional dimensions are large or if the surface scattering is completely specular then  $g_{ph}(p_{ph}, \tau_{ph}, v_{\beta}, a, b) \approx 0$  and  $\kappa_{ph}$  approaches the well-known bulk value,

$$\kappa_{phbulk} = \frac{k_B^4}{2\pi^2 \hbar^3 v_{\beta}} T^3 \int_0^{\Theta_D/T} \left[ \tau_{ph}(s) \frac{s^4 e^s}{(e^s - 1)^2} \right] ds, \quad (\text{A6})$$

where  $\bar{v}_{\beta}$  is the average group velocity of phonons.

We now summarize the computation of the electronic part of the thermal conductivity of thin nanowires. Let  $\lambda_e$  be the electron mean-free path,  $d_g$  the average grain size,  $R$  the grain-boundary reflectivity coefficient, and  $p_e$  the specular coefficient for electron scattering at the free surface. Then the electronic thermal conductivity due to the size dependence in a rectangular wire of thickness  $a$  and width  $b$  is given by

$$\kappa_e = \frac{k_B^2 k_F^2 T}{9\hbar} \lambda_e^{\nabla T} [\Phi(\alpha) - g_e(p_e, \alpha, \gamma_a, \gamma_b)], \quad (\text{A7})$$

where the size-dependent correction term  $g_e(p_e, \alpha, \gamma_a, \gamma_b)$  is given by

$$\begin{aligned} g_e(p_e, \alpha, \gamma_a, \gamma_b) &= \frac{1}{\gamma_a \gamma_b} \int_0^{\gamma_b} \int_0^{\gamma_a} \left\{ \int_{\theta_1}^{\theta_2} S_e \left( p_e, \alpha, \frac{-y}{\sin \theta'}, \frac{-\gamma_b}{\sin \theta} \right) d\theta \right. \\ &\quad + \int_{\theta_2}^{\theta_3} S_e \left[ p_e, \alpha, \frac{(\gamma_a - x)}{\cos \theta}, \frac{\gamma_a}{\cos \theta} \right] d\theta \\ &\quad + \int_{\theta_3}^{\theta_4} S_e \left[ p_e, \alpha, \frac{(\gamma_b - y)}{\sin \theta}, \frac{\gamma_b}{\sin \theta} \right] d\theta \\ &\quad \left. + \int_{\theta_4}^{\theta_1} S_e \left( p_e, \alpha, \frac{-x}{\cos \theta'}, \frac{-\gamma_a}{\cos \theta} \right) d\theta \right\} dx dy \end{aligned} \quad (\text{A8})$$

with

$$\begin{aligned} S_e(p_e, \alpha, q, r) &= (1 - p_e) \frac{3}{2\pi} \int_0^{\pi/2} \frac{\sin \phi \cos^3 \phi}{\cos \phi + \alpha} \left( \frac{e^{q/\Gamma \sin \phi}}{1 - p_e e^{r/\Gamma \sin \phi}} \right) d\phi \\ &= (1 - p_e) \frac{3}{2\pi} \int_1^{\infty} \Gamma \left( \alpha, \frac{\sqrt{u^2 - 1}}{u} \right) \frac{\sqrt{u^2 - 1}}{u^4} \left( \frac{e^{qu/\Gamma}}{1 - p_e e^{ru/\Gamma}} \right) du \end{aligned} \quad (\text{A9})$$

and  $\Gamma(\alpha(\lambda_e), |\cos \phi|) = |\cos \phi| / (\alpha(\lambda_e) + |\cos \phi|)$ , and geometric parameters

$$\begin{aligned} \theta_1 &= \arctan \frac{\gamma_b - y}{\gamma_a - x}, & \theta_2 &= \pi - \arctan \frac{\gamma_b - y}{x}, \\ \theta_3 &= \pi + \arctan \frac{y}{x}, & \theta_4 &= -\arctan \frac{y}{\gamma_a - x}. \end{aligned}$$

The definitions of  $\Phi(\alpha)$ ,  $\alpha(\lambda_e)$ ,  $\gamma_a$ , and  $\gamma_b$  are as given in Sec. II. For thin films, it can be shown that the term  $g_e(p_e, \alpha, \gamma_a)$  is given by the following expression, originally derived by Fuchs:<sup>2</sup>

$$\begin{aligned} g_e(p_e, \alpha, \gamma_a) &= (1 - p_e) \frac{6}{\pi \gamma_a} \left( \int_0^{\pi/2} \int_0^{\pi/2} \frac{\cos \theta \sin^2 \phi \cos^3 \phi}{\cos \phi + \alpha} \right. \\ &\quad \left. \times \left( \frac{1 - e^{-\gamma_a/\Gamma \sin \phi \cos \theta}}{1 - p_e e^{-\gamma_a/\Gamma \sin \phi \cos \theta}} \right) d\phi d\theta \right). \end{aligned} \quad (\text{A10})$$

\*Corresponding author; nenad.stojanovic@ttu.edu

<sup>1</sup>D. G. Cahill, W. K. Ford, K. E. Goodson, G. D. Mahan, A. Majumdar, H. J. Maris, R. Merlin, and S. R. Phillpot, *J. Appl. Phys.* **93**, 793 (2003).

<sup>2</sup>K. Fuchs, *Proc. Cambridge Philos. Soc.* **34**, 100 (1938).

<sup>3</sup>E. H. Sondheimer, *Adv. Phys.* **50**, 499 (2001).

<sup>4</sup>A. F. Mayadas and M. Shatzkes, *Phys. Rev. B* **1**, 1382 (1970).

<sup>5</sup>M. N. Ou, T. J. Yang, S. R. Harutyunyan, Y. Y. Chen, C. D. Chen, and S. J. Lai, *Appl. Phys. Lett.* **92**, 063101 (2008).

<sup>6</sup>Q. G. Zhang, B. Y. Cao, X. Zhang, M. Fujii, and K. Takahashi, *J.*

- Phys.: Condens. Matter* **18**, 7937 (2006).
- <sup>7</sup>P. Nath and K. L. Chopra, *Thin Solid Films* **20**, 53 (1974).
- <sup>8</sup>G. K. White and R. J. Tainsh, *Phys. Rev.* **119**, 1869 (1960).
- <sup>9</sup>C. L. Tien, B. F. Armally, and P. S. Agannathan, *Proceedings of Eighth Conference on Thermal Conductivity* (Plenum Press, New York, 1969), p. 13.
- <sup>10</sup>A. F. Mayadas, *J. Appl. Phys.* **39**, 4241 (1968).
- <sup>11</sup>X. Lü, W. Z. Shen, and J. H. Chu, *J. Appl. Phys.* **91**, 1542 (2002).
- <sup>12</sup>P. G. Klemens and R. K. Williams, *Int. Met. Rev.* **31**, 197 (1986).
- <sup>13</sup>B. Feng, Z. X. Li, and X. Zhang, *Thin Solid Films* **517**, 2803 (2009).
- <sup>14</sup>P. Heino and E. Ristolainen, *Microelectron. J.* **34**, 773 (2003).
- <sup>15</sup>Y. Zhou, B. Anglin, and A. Strachan, *J. Chem. Phys.* **127**, 184702 (2007).
- <sup>16</sup>N. Stojanovic, J. M. Berg, D. H. S. Maithripala, and M. Holtz, *Appl. Phys. Lett.* **95**, 091905 (2009).
- <sup>17</sup>J. M. Ziman, *Electrons and Phonons* (Oxford University Press, London, 1960).
- <sup>18</sup>S. G. Walkauskas, D. A. Broido, K. Kempa, and T. L. Reinecke, *J. Appl. Phys.* **85**, 2579 (1999).
- <sup>19</sup>J. Zou and A. Balandin, *J. Appl. Phys.* **89**, 2932 (2001).
- <sup>20</sup>G. A. Slack and S. Galginaitis, *Phys. Rev.* **133**, A253 (1964).
- <sup>21</sup>L. A. Girifalco and K. Kniaz, *J. Mater. Res.* **12**, 311 (1997).
- <sup>22</sup>W. H. Butler and R. K. Williams, *Phys. Rev. B* **18**, 6483 (1978).
- <sup>23</sup>W. Zhang, S. H. Brongersma, O. Richard, B. Brijs, R. Palmans, L. Froyen, and K. Maex, *Microelectron. Eng.* **76**, 146 (2004).
- <sup>24</sup>F. Volklein and T. Starz, *Proceedings of the 16th International Conference on Thermoelectrics*, Dresden, Germany, 1997, p. 711.
- <sup>25</sup>B. T. Boiko, A. T. Pugachev, and V. M. Bratsychin, *Thin Solid Films* **17**, 157 (1973).
- <sup>26</sup>T. M. Tritt, *Thermal Conductivity: Theory, Properties, and Applications* (Kluwer, New York, 2004).
- <sup>27</sup>Y. Hanaoka, K. Hinode, K. Takeda, and D. Kodama, *Mater. Trans.* **43**, 1621 (2002).
- <sup>28</sup>J.-W. Lee, J. K. Kim, S.-H. Kim, H.-J. Sun, H.-S. Yang, H. C. Sohn, and J. W. Kim, *Jpn. J. Appl. Phys.* **43**, 8007 (2004).
- <sup>29</sup>B. Feng, Z. Li, and X. Zhang, *J. Appl. Phys.* **105**, 104315 (2009).